Article

Hydrologic Sensitivity of a Critical Turkish Watershed to Inform Water Resource Management in an Altered Climate

Furkan Yunus Emre Cevahir [1,*], Jennifer C. Adam [2], Mingliang Liu [2] and Justin Sheffield [3]

1   Graduate School of Natural and Applied Sciences, Middle East Technical University, 06800 Ankara, Turkey
2   Department of Civil and Environmental Engineering, Washington State University, Pullman, WA 99163, USA;
    jcadam@wsu.edu (J.C.A.); mingliang.liu@wsu.edu (M.L.)
3   School of Geography and Environmental Science, University of Southampton, Southampton SO17 1BJ, UK;
    justin.sheffield@soton.ac.uk
*   Correspondence: f.yunusemre@gmail.com

Abstract: This study introduces a novel sensitivity analysis approach to assess the resilience and susceptibility of hydrologic systems to the stresses of climate change, moving away from conventional top-down methodologies. By exploring the hydrological sensitivity of the upper Kızılırmak River basin using the Variable Infiltration Capacity (VIC) hydrologic model, we employed a sensitivity-based approach as an alternative to the traditional Global Climate Model (GCM)-based methods, providing more insightful information for water managers. Considering the consistent projections of increasing temperature over this region in GCMs, the hydrologic system was perturbed to examine gradients of a more challenging climate characterized by warming and drying conditions. The sensitivity of streamflow, snow water equivalent, and evapotranspiration to temperature (T) and precipitation (P) variations under each perturbation or "reference" climate was quantified. Results indicate that streamflow responds to T negatively under all warming scenarios. As the reference climates become drier, streamflow sensitivity to P increases, indicating that meteorological drought impacts on water availability could be exacerbated. These results suggest that there will be heightened difficulty in managing water resources in the region if it undergoes both warming and drying due to the following setbacks: (1) water availability will shift away from the summer season of peak water demand due to the warming effects on the snowpack, (2) annual water availability will likely decrease due to a combination of warming and lower precipitation, and (3) streamflow sensitivity to hydroclimatic variability will increase, meaning that there will be more extreme impacts to water availability. Water managers will need to plan for a larger set of extreme conditions.

Keywords: hydrologic sensitivity; variable infiltration capacity model; climate change

1. Introduction

Freshwater is a critical resource for all life forms; however, its availability in space and time is being affected by climate change, often in detrimental ways. For example, in snowmelt-dominant watersheds, warming-induced depletions of the seasonal snowpack result in a shift of water availability away from the summer season of peak water use [1–3]. Also, Adam et al. [4] concluded that projected losses in the snowpack and warm-season runoff are linked to warming temperatures in snow-dominated regions. These studies of hydrological impacts of climate change were studied by many authors in the past [5–8].

To analyze the hydrological risks caused by climate change, the model's climate information is collected from Global Climate Models (GCMs), which generally have coarse spatial resolutions (150–200 km). The necessity to convert inputs to a hydrological model, which runs at a higher spatial resolution than GCMs, is one of the major challenges for such studies. For example, modeling a watershed in regions with complex topography can result in significant uncertainties even though downscaling techniques are utilized. Due to the uncertainties of GCM-based analyses, hydrological models have been run based on

some reference climates (please see the hydrological impact figures of simulated change at 1.5 °C, 2 °C, and 4 °C reference climates in the *IPCC 6th Assessment Report* [9]). Hydrological projection studies using such reference climates adopt the general results of GCMs. Using climate information as an input or using GCMs as a contribution to climate information in risk analysis reveals two different approaches. Two methods, "top-down" and "bottom-up", generally used in the hydrological risk analysis, are briefly mentioned below.

The methods of "top-down" and "bottom-up" have been used to assess the hydrological vulnerability of basins by employing climate projections. The top-down method, also known as the scenario-led or GCM-based approach, selects one or more GCMs based on multiple greenhouse gas emission scenarios and uses downscaling methods and hydrological models to predict changes and potential vulnerabilities of water resource systems. This method has some limitations because of the significant uncertainties associated with GCMs, downscaling techniques, and greenhouse gas emissions. Wilby & Dessai [10] demonstrate that there is an expanding envelope of uncertainty that arises in the top-down approach, as the uncertainty increases from understanding the role of the future society in climate change to adaptation responses. Hallegatte [11] states that this degree of uncertainty makes it difficult for decision-makers to adapt to climate change through long-term investments. Moreover, because of the computational requirements associated with running a large set of GCMs under different greenhouse gas scenarios, it is impractical to examine the full range of possible future climatic conditions.

The bottom-up method, also known as the sensitivity-based approach, identifies the most sensitive conditions of water resource systems to determine critical conditions and predict how water resource systems will respond to a wide range of possible climatic conditions. With this method, a wider range of future climate forecasts can be identified from climate projections. Then, at the end of the sensitivity analysis, decision-makers can observe climatic conditions under which the coping thresholds of the water resource system will be strained. As an alternative to the GCM-based approach in the analyses of risk assessments, Brown & Wilby [12] elaborate on the advantage of the better insight that the sensitivity analysis method provides to decision-makers. A comparison of the limitations and the advantages of these two methods was provided by Nazemi & Wheater [13].

Vano et al. [14] applied the sensitivity-based approach to examine streamflow response to changes in precipitation and temperature in the Colorado River basin. They compared these sensitivities for multiple altered "reference" climates and found that these sensitivities change as a function of reference climate, indicating that climate change can affect not only mean streamflow values but also how sensitive they are to climate variations. As a follow-on study, Vano & Lettenmaier [15] compared a sensitivity-based (bottom-up) approach to the GCM-driven (top-down approach) to understanding streamflow vulnerability to climate change and argued that the sensitivity-based approach produces viable first-order predictions that can easily be applied to newly released climate information.

Using the top-down approach as described above, the study area, the Kizilirmak River basin (KRB) has been analyzed by several climate projections and hydrological model analyses. Using a regional climate model (RegCM3) [16], Önol et al. [17] spatially downscaled climate projections from three GCMs under the scenarios of A2, A1FI, and B1, to the end of the 21st century over the Black Sea and eastern Mediterranean regions. Also, using dynamic downscaling methods (RegCM4), a study on the climate projections of the KRB was carried out by the Turkish General Directorate of Water Management under a project on the impact of climate change on water resources in Turkey's rivers [18,19]. Overall, the study revealed that the basin would be affected by climate change, driven by the projected increase in temperature and, notably, the projected variations in precipitation, encompassing both increases and, more prominently, decreases. As an alternative, this sensitivity-based (i.e., "bottom-up") approach can provide decision-makers more insight into risk assessments.

In this study, the sensitivity framework established by Vano et al. [14] was applied to assess the risks caused by climate change to water management in the headwater section of the Kizilirmak River. This river drains the second largest area of all basins in Turkey and is an important water source for the energy, water, and food needs of approximately 5 million inhabitants [20]. This watershed, being a snowmelt-dominant system, is potentially vulnerable to a warming climate since warming can cause more precipitation to fall as rain and earlier snowmelt, therefore shifting water availability away from the summer season of peak water demand. Unfortunately, Global Climate Models (GCMs) are projecting warming temperatures and reduced annual precipitation in this region, both of which will exacerbate existing management challenges or create new conditions of water scarcity, particularly during the summer [21]. This study focuses on the headwater section of the KRB, the Upper Kızılırmak River basin (UKRB), because much of the water supply is generated from the UKRB, which is snow-dominant.

In this study, we adopted a novel sensitivity analysis approach rather than the conventional top-down method to examine the impact of climate change on the hydrologic system. Through this method, we aimed to understand how resilient or susceptible the hydrologic system is to various strains induced by climate change. Given the absence of the prior application of the hydrological sensitivity analysis approach within the specified region, two research questions were posed:

(1) What are the long-term hydrologic effects of realistic ranges of projected temperature and precipitation changes in the UKRB?
(2) How does the hydrological sensitivity of the basin vary across changes in temperature and precipitation (i.e., across reference climates)?

To address these questions, we performed the following tasks to answer these questions: implement, calibrate, and evaluate a semi-distributed hydrological [22] model over the UKRB; investigate the sensitivity of the UKRB hydroclimatology to possible future changes in temperature and precipitation; quantify the UKRB streamflow sensitivity to precipitation and temperature for multiple reference climates; and discuss the implications of the UKRB hydrologic changes and sensitivities to water resource management in the entire basin.

2. Materials and Methods

2.1. Study Area

2.1.1. Upper Kızılırmak River Basin (UKRB)

The study area (Figure 1) constitutes a drainage area of about 16,500 km^2, which is mostly in the Upper Kızılırmak River basin (UKRB). The river originates from Kızıldağ, east of Sivas, and flows first to the west and then to the southwest until Avanos and then heads to the northwest [23] (Figure 1). The study area's drainage basin extends to the vicinity of the Yamula Dam, which was constructed and opened in 2005. Behind the Dam, there is a streamflow observation station whose data was used for hydrological model calibration and evaluation, as illustrated in Figure 1. The UKRB belongs to continental climate zones, and the precipitation during the winter season is not as much as in the spring, while most of the annual total precipitation occurs in these two seasons since, during the summertime, a tropical dry and hot air mass coming from the south controls Central Anatolia [23].

From a hydrological perspective, streamflow is dominated by winter and spring precipitation, which occurs mostly as snow in high altitudes and is the source of the spring freshet that is responsible for most of the river's annual streamflow (Figure 2). As Sağdıç and Koç [23] reported, the number of days with snow cover significantly decreases in April when streamflow reaches its maximum rate. As shown in Figure 2, precipitation and streamflow reached maximum values (3.2 mm/day and around 228.7 cms (cubic meter per second)) in April. From autumn until the end of winter, precipitation and streamflow values increased from about 1.62 mm/day (17.64 cms) to 2.1 mm/day (49 cms). Streamflow values decreased after mid-April and reach their lowest values (15.52 cms) during the summer.
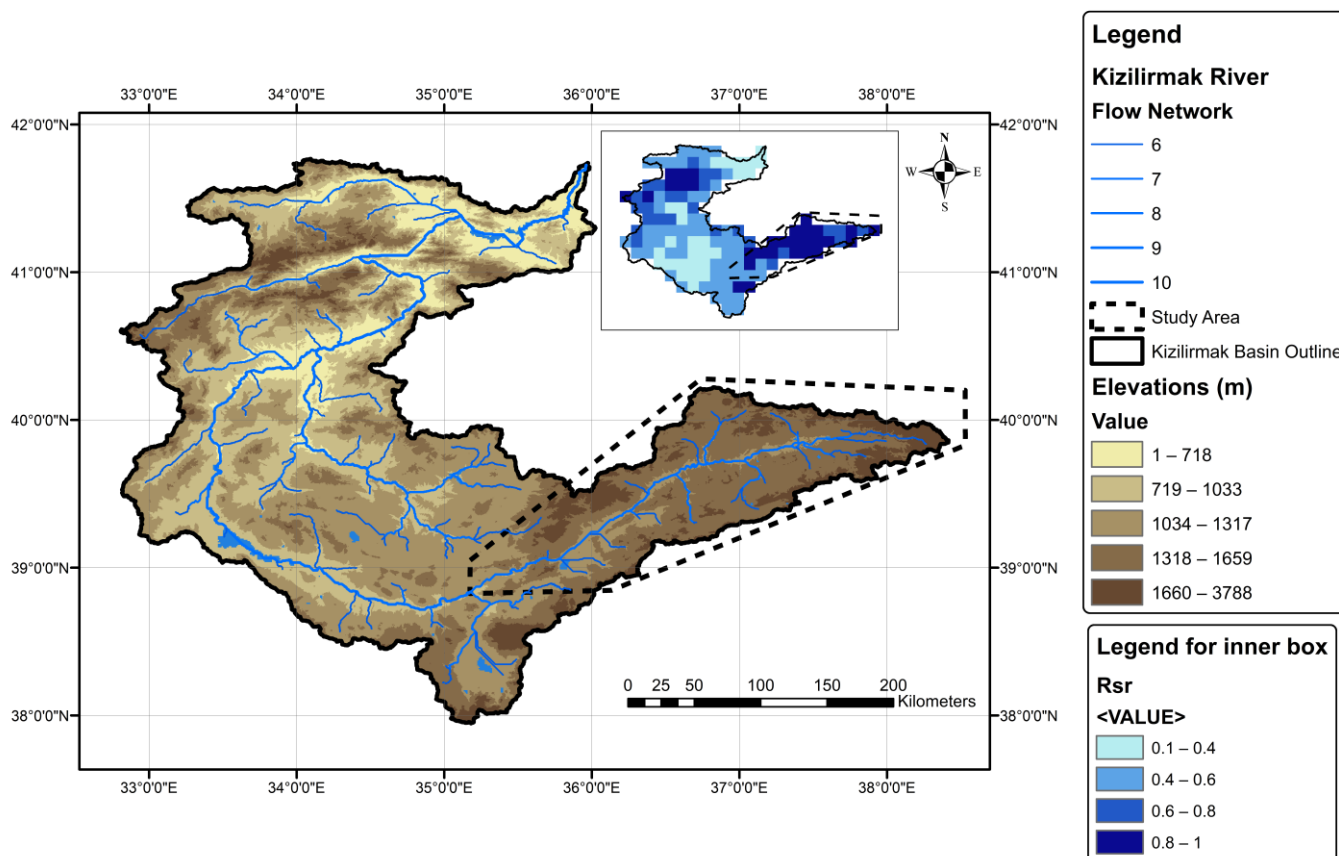
Figure 1. Map of study domain. Solid line boundary: the Kızılırmak River basin; dashed line boundary: the Upper Kızılırmak River basin, which is the study area; the brown gradient color of the main plot shows the elevation; and the inset plot with gradient blues show the RSR ratio (ratio of snow contribution to runoff—see Section 2.4 for Methods).

2.1.2. Previous Research Activities on Climate Impact over KRB

The coarse resolution CMIP5 (Coupled Model Intercomparison Project) projections indicate that in Turkey, by the end of the 21st century (relative to the means of 1986–2005), an increase of the surface temperature is expected to be between 0.5 and 1 °C and 4 and 5 °C degrees for the RCP4.5 (Representative Concentration Pathways) and RCP8.5 scenarios, respectively. At the same time, precipitation is projected to decrease by up to 10 percent and 30 percent for RCP4.5 and RCP8.5, respectively [27–29].

When the region of the KRB is specifically analyzed from the simulation maps in the studies, by 2100, the surface temperatures for all seasons are estimated to increase, according to all emission scenarios and three climate models [16,17]. In addition, the models agree that winter precipitation will increase along the coast of the Black Sea in the basin. Summer precipitation will decrease significantly throughout most of the basin. There will be a decrease in precipitation in the inland areas where the continental climate is dominant.

In the KRB, projections for temperature, precipitation, and surface runoff were made at a resolution of 10 × 10 km for RCP4.5 and RCP8.5 scenarios by dynamically downscaling three GCMs (HadGEM2-ES, MPI-ESM-MR, and CNRMCM5.1) using RegCM4.3 [18,19]. Based on the reference years of 1971–2000, increases in basin-average temperature for the years 2041–2050 are between 1.1 and 2.3 °C degrees for RCP4.5 and 1.5 and 2.8 °C for RCP8.5. Precipitation is projected to change between 5.8% and −3.4% for RCP4.5 and between 2.8% and −2.5% for RCP8.5. Among all 30-year averages, for the period of 2041–2070, the decrease in the total surface runoff in the basin is projected to be maximum at 54%.
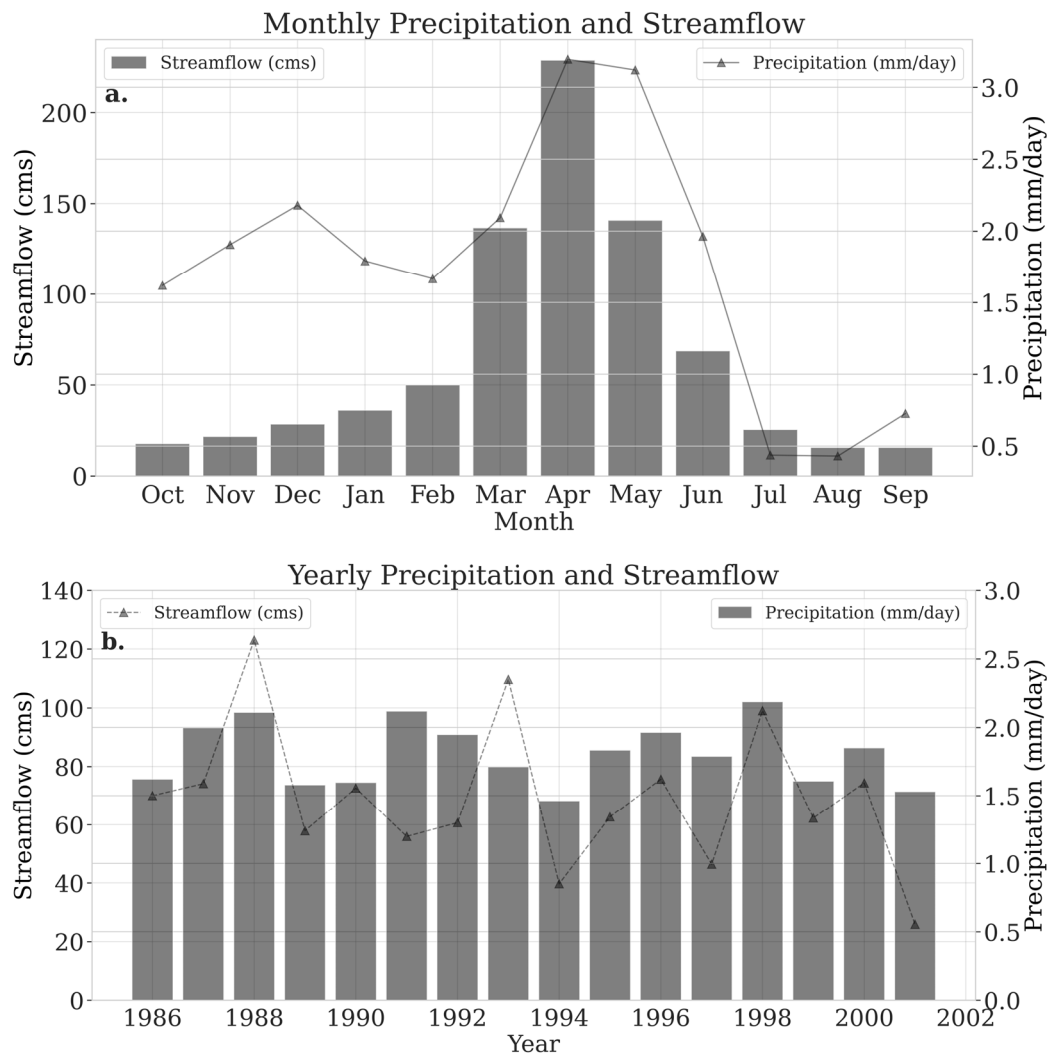
Figure 2. Monthly average of daily precipitation and observed streamflow across the Upper Kızılır-mak River from 1986 to 2001 (**a**), as well as the annual average precipitation and observed streamflow for the basin during the same period (**b**). The observed streamflow is obtained from "DSİ General Directorate—Streamflow Observation Annuals" [24], and precipitation data were computed from the global meteorological forcing dataset [25] and multiplied by the orographic correction factor for the study area (1.45). The correction factors are globally available [26].

As seen from the projection studies mentioned in this section, the GCMs' projections of temperature and precipitation vary substantially. In the GCM-based method (the top-down method), the risk assessment relies on the accuracy of the projections; however, in the sensitivity-based approach (the bottom-up method), it is more important to analyze hydrologic sensitivities under potentially harmful warming and drying climatic conditions. Therefore, for this study, temperatures are increased up to 1.5 °C, and precipitation is decreased by up to 70%.

2.2. Model Descriptions

The Variable Infiltration Capacity (VIC) model, a macroscale hydrological model that integrates the parameters of meteorological, vegetation, and soil properties to solve water and energy balances in space and time, has been used in this study (version 4.1.2) [22,30,31]. Detailed descriptions of the model structure, equations, and snowpack-related hydrological processes can be found in [4,22,30,32,33]. To understand the critical consequences of climate change on water resources and to evaluate the hydrological effects of climate change on a wide range of watersheds, the VIC model has been updated and improved during the

last decades (detailed information can be found at https://vic.readthedocs.io/en/master/, accessed on 1 January 2024). VIC has been applied at regional scales [1,34–37] and global scales [4,38,39]. It has also been coupled with a crop model (VIC-CropSyst) to assess the agricultural impacts of climate change [40–43]. In addition, it has been used for hydrological sensitivity analyses [15,44–48].

2.3. Data Sources

Soil data, estimated using the VIC model studies; leaf area index, estimated using radiative transfer models; and vegetation library were obtained from global datasets available at https://vic.readthedocs.io/en/master/Datasets/Datasets/, accessed on 1 January 2024 [49–51] (please also see data availability statement). These data have been updated and rendered at a finer spatial resolution of $0.25° \times 0.25°$ by Justin Sheffield (https://hydrology.soton.ac.uk/, accessed on 1 January 2024) [39], which we used for this study. Daily meteorological input data (maximum temperature (T_{max}), minimum temperature (T_{min}), wind speed, and precipitation) were obtained from Justin Sheffield [25,52]. Sheffield et al. published the global meteorological dataset, which has been utilized in numerous climate and hydrological studies [53–55]. The dataset combines global observational meteorological data with NCEP-NCAR (National Centers for Environmental Prediction–National Center for Atmospheric Research) reanalysis, addressing biases in precipitation and near-surface meteorology. Corrections use observation-based data for precipitation, temperature, and radiation, as well as adjusting rain day statistics. Wind-induced underestimation of solid precipitation is fixed with WMO (World Meteorological Organization) findings. Precipitation data were spatially downscaled using the GPCP (Global Precipitation Climatology Project) daily product.

Due to the prevalence of mountainous terrain in the UKRB, precipitation data were multiplied by a correction factor of 1.45 to account for orographic effects. This correction was made to compensate for potential deficiencies in observed precipitation amounts due to the topographic complexity of the basin. Adam et al. published these correction factors globally [26]. Digital elevation information needed for the routing model was obtained from the Shuttle Radar Topography Mission (SRTM) at a 90 m resolution.

2.4. Calibration

After the routing process, calibration and evaluation processes were performed sequentially. The calibration period ranged from 1950 to 1975, while the evaluation period spanned from 1976 to 2001. The automated multi-objective optimization calibration ("MOCOM-UA") was implemented to calibrate the watershed [56]. The optimization of model parameters, namely bi (variable infiltration curve), Ds (velocity of baseflow), Ws (fraction of maximum soil moisture where non-linear baseflow occurs), and Dsmax (maximum velocity of baseflow), was conducted within the framework of MOCOM-UA (Table 1; [57]). Six metrics/objectives were selected: (1) Nash-Sutcliff model efficiency coefficient (NSE) (Equation (1)); (2) Nash–Sutcliffe efficiency with logarithmic values (Ln NSE; (3) relative bias; (4) coefficient of determination r2; (5) absolute average peak flow difference; and (6) root mean square error (RMSE) (Appendix A). After obtaining the Pareto optimal solutions, we selected the soil parameter set with maximum NSE as the final calibration product. The calibration was carried out using streamflow observations from the observation station located in the village of Yamula, near the Yamula dam (station code: E15A001, latitude: 38.888°, longitude: 35.257°) (Figure 1). The period for the calibration was 1950–1975, during which no human-made upstream reservoirs existed (Figure 3 and Table 2). As listed in Table 2, some reservoirs were opened during the evaluation period (1976–2001), which may affect the evaluation results. Table 1 provides parameter ranges and the final calibration parameter values used for VIC, as well as the descriptions of the parameters. Detailed information about the soil parameter calibration and the calibration ranges of the soil parameters can be accessed at https://vic.readthedocs.io/en/vic.4.2.d/Documentation/CalibrateSoil/, accessed on 1 January 2024.

Table 1. Calibration parameters used for VIC and their descriptions (the ranges are from Maurer et al. [57]).

Calibration Parameters	Description of the Parameters	Parameter Range	Calibrated Value
b-infilt (unitless)	Used to define the shape parameter of the VIC curve. Higher values will produce more runoff.	0.001 to 0.3	0.16
Ds (fraction)	Ds represents the fraction of the Dsmax parameter at which non-linear baseflow occurs.	1×10^{-5} to <1	0.69
Ds,max (mm/day)	Ds,max is the maximum velocity of baseflow for each grid cell.	0.01 to 30	14.40
Ws (fraction)	Ws is the fraction of maximum soil moisture where non-linear baseflow occurs. An increase of Ws will delay runoff peaks.	0.05 to 1	0.63
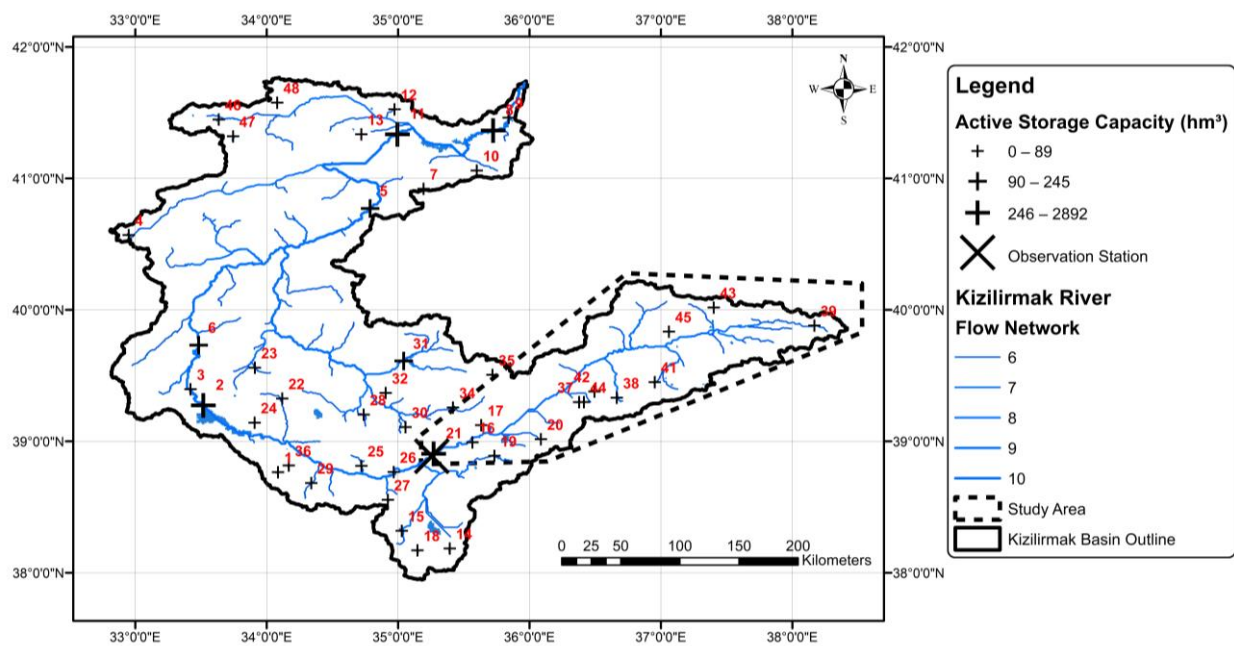
Figure 3. Reservoirs (active storage capacities—hm^3) with their object ids (see Table 2 to check their associated names inside study area) in the KRB. The location of the observation station and the study area are shown in the figure. The reservoir information was received from the DSI (Turkish Directorate General for State Hydraulic Works).

Table 2. Shows the reservoirs upstream of the observation station used for calibration. The reservoirs with the asterisk sign were built during the model evaluation period (i.e., 1976–2001). (Note: no reservoirs were constructed before or during the model calibration period (i.e., 1950–1975).

Reservoir Name (Obj. ID)	Open Year	Active Capacity (Million Cubic Meters)
* Aksaklı-Karaçalı (16)	1994	9.4
Kayapınar (17)	2013	3.0
Sarıoğlan (20)	2006	20.4
Çermikler (37)	2013	6.9
* Gazibey (38)	1992	21.3
Karacalar (41)	2008	39.6
* Maksutlu (42)	1982	1.6
Pusat Özen (43)	2009	89.3
* Yapı Altın (44)	1986	10.6
Imranlı (39)	2003	57.3
4 Eylül (45)	2006	80.4
Yamula (21)	2005	2076.0

To evaluate VIC model results, *NSE* (Nash and Sutcliffe [58] and *RMSE* (root mean square error) observations standard deviation ratio (*RSR*) (Singh et al. [59] were used. *NSE* is defined by (Equation (1)):

$$NSE = 1 - \frac{\sum_{t=1}^{T} \left(\hat{Y}_i^t - Y_o^t \right)^2}{\sum_{t=1}^{T} \left(Y_o^t - \overline{Y}_o \right)^2} \tag{1}$$

where *NSE* is the Nash–Sutcliffe coefficient; $\hat{Y}_i^t$ is simulated flow; Y_o^t is the observed streamflow; and $\overline{Y}_o$ is the annual average observed streamflow. *RSR* is defined by (Equation (2)):

$$RSR = \frac{RMSE}{STDEV_{obs}} = \frac{\left[\sqrt{\sum_{i=1}^{n} \left(Y_i^{obs} - Y_i^{sim} \right)^2} \right]}{\left[\sqrt{\sum_{i=1}^{n} \left(Y_i^{obs} - Y^{mean} \right)^2} \right]} \tag{2}$$

where *RSR* is *RMSE* observations standard deviation ratio; Y_i^{obs} is observed flow; Y_i^{sim} is simulated flow; and Y^{mean} is the average flow. The calibration and evaluation statistics are provided in the Results, Section 3.1.

2.5. Quantification of Ratio of Snowmelt Contribution to Runoff Generation (R_{SR})

To examine the dependence of the runoff on snowmelt in the UKRB, a ratio of snowmelt contribution to runoff generation (R_{SR}) was quantified for each water year (Equation (3)) [60,61]:

$$R_{SR} = \frac{SWE_{melt}}{\sum_{t=1}^{N} R_t} \tag{3}$$

where *R* is runoff (mm/day), and *N* is 365 (nonleap year) or 366 (leap year); *t* = 1 marks 1 October of the given year; and SWE_{melt} is calculated as (Equation (4)):

$$SWE_{melt} = SWE_{max} - SWE_{min} \tag{4}$$

where SWE_{max} is the maximum snow water equivalent of the year, and SWE_{min} is the minimum snow water equivalent of the year. Snow water equivalent and total runoff are the outputs of the VIC simulation for the years between 1950 and 2016, and the average R_{SR} was calculated during these years.

Figure 4 presents a flowchart that illustrates the stages and components of the study. To see how perturbed the forcing data and related formulations please check Section 2.7.

2.6. Generation of Reference Climate for Sensitivity Analysis

We applied the sensitivity framework described by Vano et al. [14], in which we sought to quantify streamflow sensitivity to precipitation and temperature for multiple reference climates to see how climate change impacts not only mean streamflow but also its sensitivity to weather variations. Thus, precipitation data were perturbed by multiplying the precipitation values by 70%, 80%, 90%, 100%, and 110%, respectively, and the temperature (Tmin and Tmax concurrently) was perturbed by increasing 0, 0.5, 1, and 1.5 °C, respectively. For each reference climate, streamflow values (Q_{ref}) were obtained by running VIC using the perturbed climate data for each reference climate.
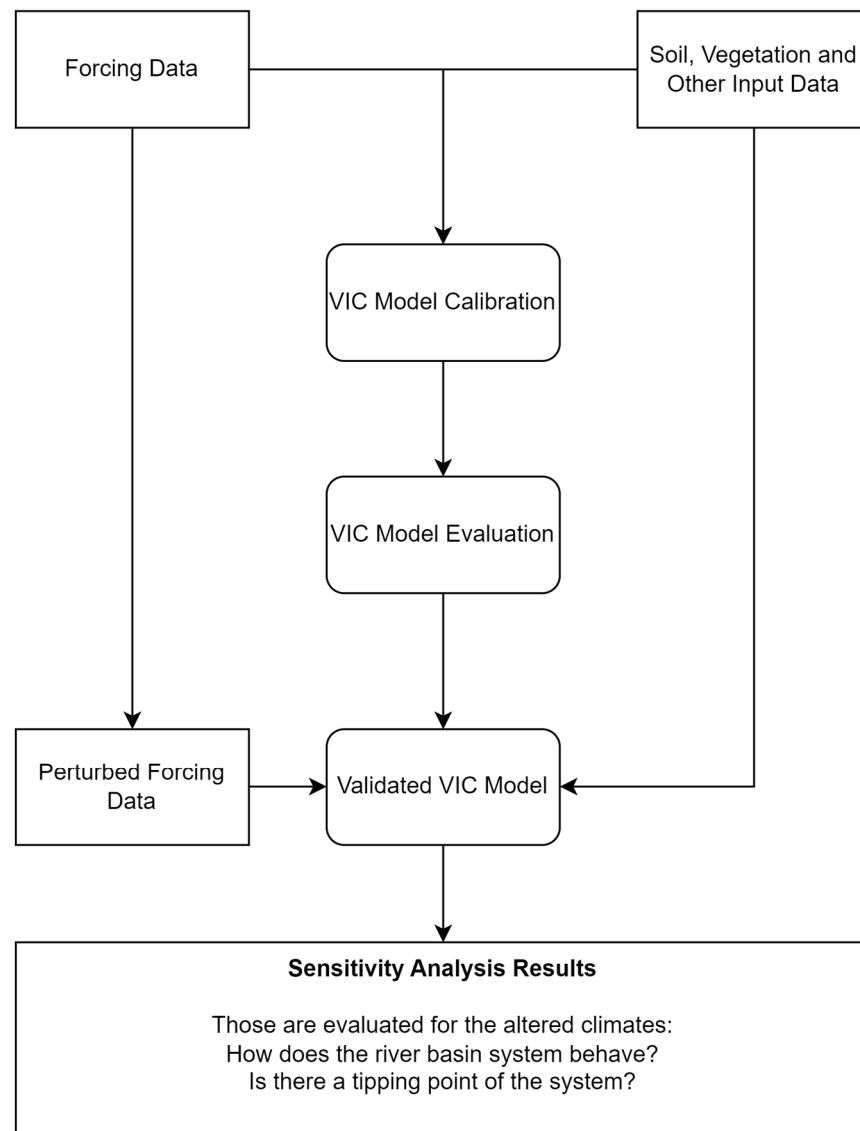
Figure 4. Flowchart of the study.

2.7. Formulations of Precipitation Elasticity and Temperature Sensitivity

Following the nomenclature of Vano et al. [14], two terms were used in the sensitivity analysis: ε_Q for streamflow (Q) elasticity to precipitation (Equation (5)) and S_Q for streamflow sensitivity to temperature (Equation (6)). ε_Q and S_Q can be defined as how an incremental change (or perturbation) in precipitation and temperature results in a percent change in streamflow.

$$\varepsilon_Q = \frac{\frac{Q_{ref+\Delta} - Q_{ref}}{Q_{ref}}}{\Delta P(\%)} \tag{5}$$

$$S_Q = \frac{\frac{Q_{ref+\Delta} - Q_{ref}}{Q_{ref}}}{\Delta T(^\circ\text{C})} \tag{6}$$

For each of the reference climates described in Section 2.5, we calculated both ε_Q and S_Q by very small increments (which are referred to as Δ) of P and T. For Δ, we use 0.1 °C for T and 1% for P to examine the sensitivity of streamflow to small increments while avoiding computational artifacts that occur if Δ is too small. The minimum and maximum temperature values were increased by the same amount (i.e., $\Delta = 0.1$ °C). In Appendix B, Tables A1 and A2 show the perturbations made to T and P (respectively) for

each reference climate and incremental change conditions to calculate Q_{ref} and $Q_{ref+\Delta}$, needed for Equations (5) and (6). Using the same methodology as was performed for streamflow, we also calculated the precipitation elasticity of snow water equivalent (*SWE*) and evapotranspiration (*ET*) (ε_{SWE} and ε_{ET}), as well as the temperature sensitivity of *SWE* and *ET* (S_{SWE} and S_{ET}). This was performed by replacing Q with either *SWE* or *ET* in Equations (5) and (6). For more details, please see Appendix B.

2.8. Budyko Curve

The Budyko curve was employed to examine whether temperature conditions influence the dryness of the conditions. According to Budyko et al. [62], there is a relationship between the evaporative index (the ratio of annual actual *ET* to annual *P*) and the aridity index (the ratio of annual potential *ET* to annual *P*). The Budyko curve, a semi-empirical expression of the coupled water-energy balance, is widely used in the hydrological analysis of catchments [63,64]. The Budyko equation is defined by (Equation (7)) [62]:

$$\frac{E_a}{P} = \left\{ \left(\frac{E_p}{P} \right) \tanh \left(\frac{1}{\left(\frac{E_p}{P} \right)} \right) \left(1 - exp^{-\left(\frac{E_p}{P} \right)} \right) \right\}^{0.5} \tag{7}$$

where E_a is annual actual *ET* (AET), E_p is annual potential *ET* (PET), *P* is annual *P*. In order to see results related to the Budyko curve, please check Section 3.4.

2.9. Formulation of Coefficient of Variation

Increases in streamflow sensitivities to temperature and precipitation may result in more variable streamflow in response to changing climate conditions. To examine this variability, The coefficient of variation (*CV*) was calculated for each reference climate on a monthly basis (Please see Section 3.5). *CV* is a useful statistical measure in comparing the degree of variation from one data series to another. *CV* is calculated by (Equation (8)):

$$CV = \frac{\sigma}{\mu} \tag{8}$$

where σ is the standard deviation, and μ is the mean. In this study, for each reference climate, *CV* is calculated by dividing the standard deviation of the monthly mean values of each year over the entire period (1971–2000) by the mean of the monthly average values of each year over the entire period (1971–2000).

3. Results

3.1. Model Performance during Calibration and Evaluation Periods

Figure 5 depicts the model performance of simulated monthly streamflow during calibration (for the period of 1950–1975; Figure 5a,c) and evaluation (for the period of 1976–2001; Figure 5b,d) periods. The NSEs are 0.78 and 0.53, and the RSRs are 0.47 and 0.69 for the calibration and evaluation periods, respectively. As shown in Table 2, the reservoirs Aksaklı, Gazibey, Yapıaltın, and Maksutlu were constructed during the evaluation period; these reservoirs have a total capacity of 42.9 million cubic meters. However, this only accounts for roughly 2% of the total annual streamflow; therefore, it is unlikely to have any significant effect on the model performance metrics during the evaluation period.

Both calibration and evaluation results show an underestimation of the magnitude of the snowmelt peak, and the evaluation results also show a mismatch in the timing of the snowmelt peak. Although the regulated streamflow by human-made reservoirs during the evaluation period might partially explain this underestimation and the shifting of the peak during the evaluation period, these biases are most likely due to an underestimation of snowfall [65] and precipitation over mountainous areas since most weather stations are located at lower elevations [26]. Although a correction factor for orographic precipitation [26] was applied in this study, we did not utilize a gridded precipitation dataset that includes

corrections to the gauges themselves. Nevertheless, according to the criteria of [66], NSEs and RSRs are "satisfactory" for this study.
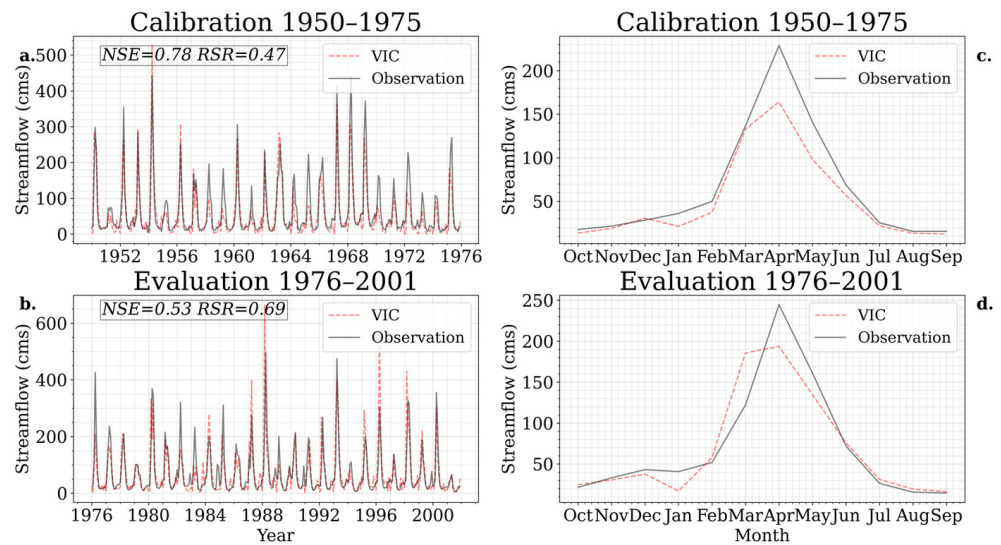

Figure 5. Comparison between observed and VIC modeled streamflow from the UKRB during both the calibration (1950–1975) and evaluation (1976–2001) periods, with panels (**a**,**b**) representing yearly and panels (**c**,**d**) representing monthly mean streamflow.

3.2. Monthly Water Balance and Effects of Climate Perturbations

Figure 6a shows the average monthly water fluxes (P, ET, and Q) as well as the hydrological state (SWE) during 1971–2000. Precipitation is above 1.6 mm/day except for July–September, its peak is in April with 3.1 mm/day, and its minimum is in August with 0.43 mm/day. ET is higher than 1 mm/day during March–July and lower than 0.5 mm/day during December–Feb. The lowest and highest monthly ET is in January, with 0.057 mm/day, and in May, with 4.53 mm/day, respectively. Streamflow (runoff + baseflow) increases starting from February, peaks in March (1036 mm/day), and decreases to a minimum in August and September (0.083 mm/day). SWE peaks in February (74.65 mm) and significantly decreases after March, which contributes substantial snowmelt to Q during March–April.

3.2.1. Impacts of Precipitation Perturbations

Figure 6b shows the response of the hydrologic fluxes and SWE to P perturbations of +10, −10, −20, and −30%. Because P was adjusted as a percent, the absolute change in the summer months (July–August) is much less than other months, which have higher P (Figure 6b). Peak Q always occurs in March with 0.36, 0.50, 0.72, 1.03, and 1.22 mm/day under 70%, 80%, 90%, 100%, and 110% reference P, respectively. Nevertheless, as the P perturbation decreases from 110 to 70%, the differences in Q from March to June are becoming less. The minimum Q occurs between August, September, and January, depending on the reference P (Figure 6b). SWE and ET are positively correlated with the reference P; i.e., higher P is generally associated with higher SWE and ET. Overall, Q significantly decreases as the reference P reduces, particularly during springtime when the streamflow peaks.
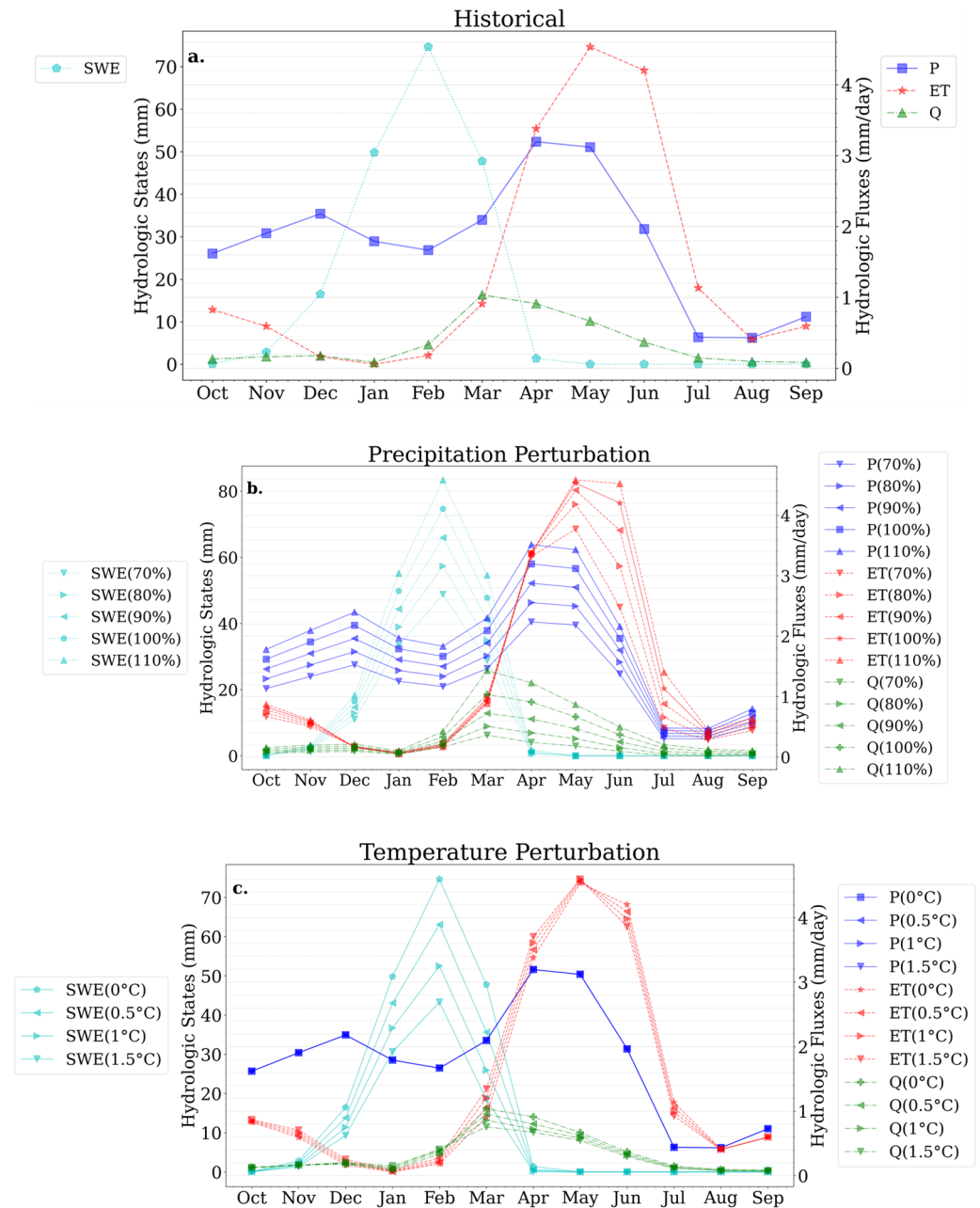
Figure 6. Sensitivities of modeled basin-average hydrologic fluxes (right axis) and SWE (left axis) to changes in the reference climates. SWE, P, ET, and Q represent snow-water equivalent, precipitation, evapotranspiration, and streamflow (i.e., runoff plus baseflow), respectively. Historical averages of the fluxes and SWE are shown in subfigure a. The averages are from 1971–2000 for months from October to September. Values are averages across all basin grid cells (not routed streamflow, although this is a small enough watershed that routing time is small and the routed flows are nearly identical to the sum of runoff and baseflow for each month). Values in the lower two rows represent changes from precipitation perturbations (**b**) of 70, 80, 90, and 110% (second row) and temperature increases (**c**) of 0.5, 1, and 1.5 °C (bottom row).

3.2.2. Impact of Temperature Perturbations

Figure 6c shows the response of the hydrologic fluxes and SWE due to T perturbations of 0.5, 1, and 1.5 °C, respectively. Warming leads to a reduction in Q during March–May, while it increases during January–February; thus, there is a small shift from early summer/later spring to late winter/early spring. Peak Q (always March) is 1.04, 0.95, 0.86, and 0.76 mm/day under 0, 0.5, 1, and 1.5 °C perturbations, respectively. The decrease

in SWE under warming is substantial during January–March when the average SWE is high. ET increases in response to warming in the springtime before May, while it decreases afterward because of early soil moisture depletion (Figure 6c).

3.3. Elasticities of Q, SWE, and ET to Precipitation and Temperature

Figure 7 shows Q, SWE, and ET elasticities to P under each P reference climate (i.e., 70, 80, 90, 100, and 110% of the historical average). As the reference climates become drier, the elasticities of Q, ET, and SWE to P all increase. However, the shape of this response is different in each case: moving towards the driest reference climates, the change in Q elasticity becomes flat, and the change in ET elasticity becomes higher, while the increase in SWE elasticity stays constant across the P perturbation gradient from wetter to drier. As the climate becomes dryer, ET will be more water-limited (see Section 3.4) and, therefore, more sensitive to changes in P.
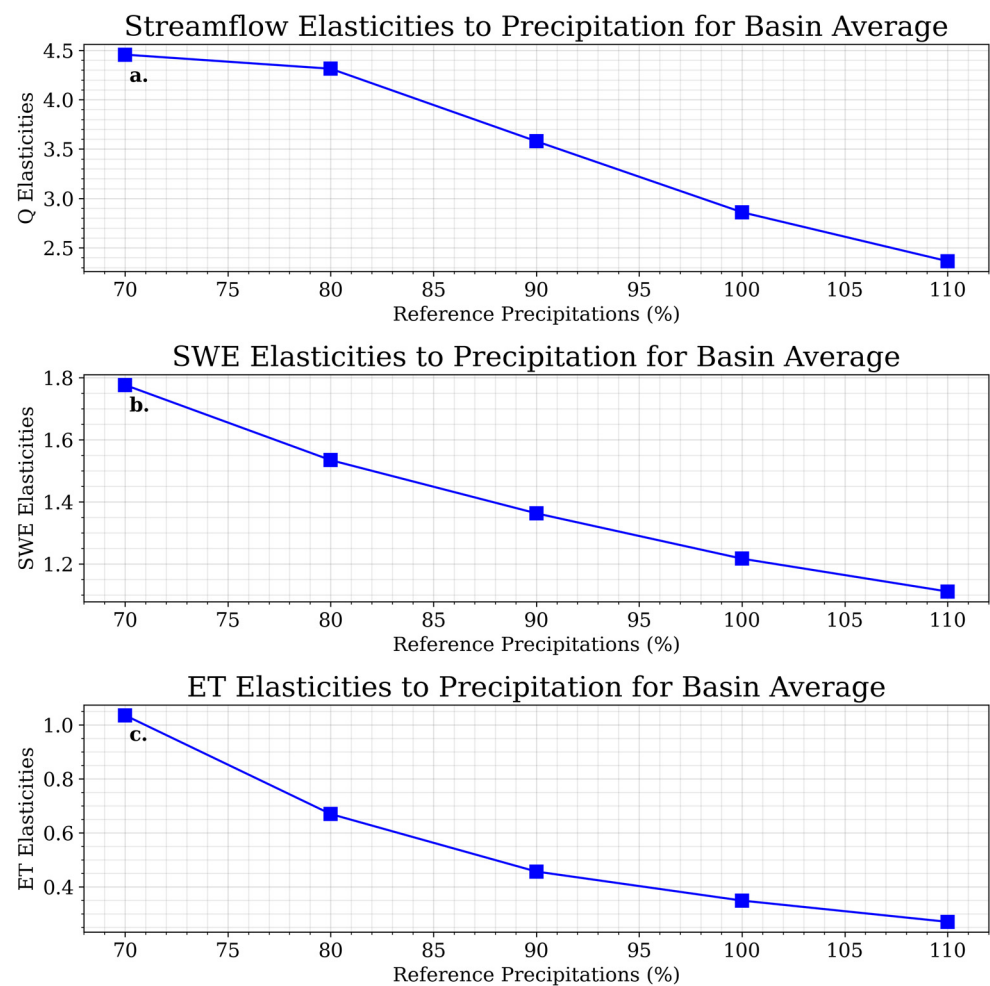

Figure 7. Streamflow, snow water equivalent, and evapotranspiration elasticities to the precipitation over reference precipitations (70, 80, 90, 100, and 110%) for the basin average. Values on the y-axis are elasticities. For example, if ε is 3, a 10% decrease in precipitation would result in a 30% decrease in streamflow. The figure shows delta perturbations and the resulting change in elasticities where percentages relate to differences in reference climate from historical.

Figure 8 shows Q, SWE, and ET sensitivities to T for each of the T reference climates. Q and SWE respond to temperature negatively, while ET is positive under all warming scenarios. Increasing T normally results in elevated ET unless the water is limiting, and thus, a decrease in Q. Similarly, an increase in T results in less snowfall, thereby reducing SWE accumulation. Unlike the monotonic response to P, the response of Q, ET, and SWE

to warming is non-monotonic. There is a "tipping point" at the 0.5 °C reference climate, which is associated with the highest (most negative) SWE sensitivity and the lowest (least negative and positive, respectively) Q and ET sensitivities. SWE is playing a major role in causing this tipping point. We hypothesize that the warming is just enough to reduce the number of winter days near the 0 °C isotherm to cause the snowpack to be highly sensitive to any additional warming but not any further since not enough snowpack is left to respond to T perturbations. This would cause the maximum negative sensitivity of SWE to T at the 0.5 °C reference climate. Similarly, ET is least sensitive to warming in this reference climate. Because of the heightened SWE sensitivity at this tipping point, any additional available energy would be utilized for melting SWE rather than for increasing ET (making ET less sensitive). Beyond the 0.5 °C reference climate, however, ET sensitivity increases with warming. This is likely due to a lengthening of the warm season, thus increasing the potential ET.
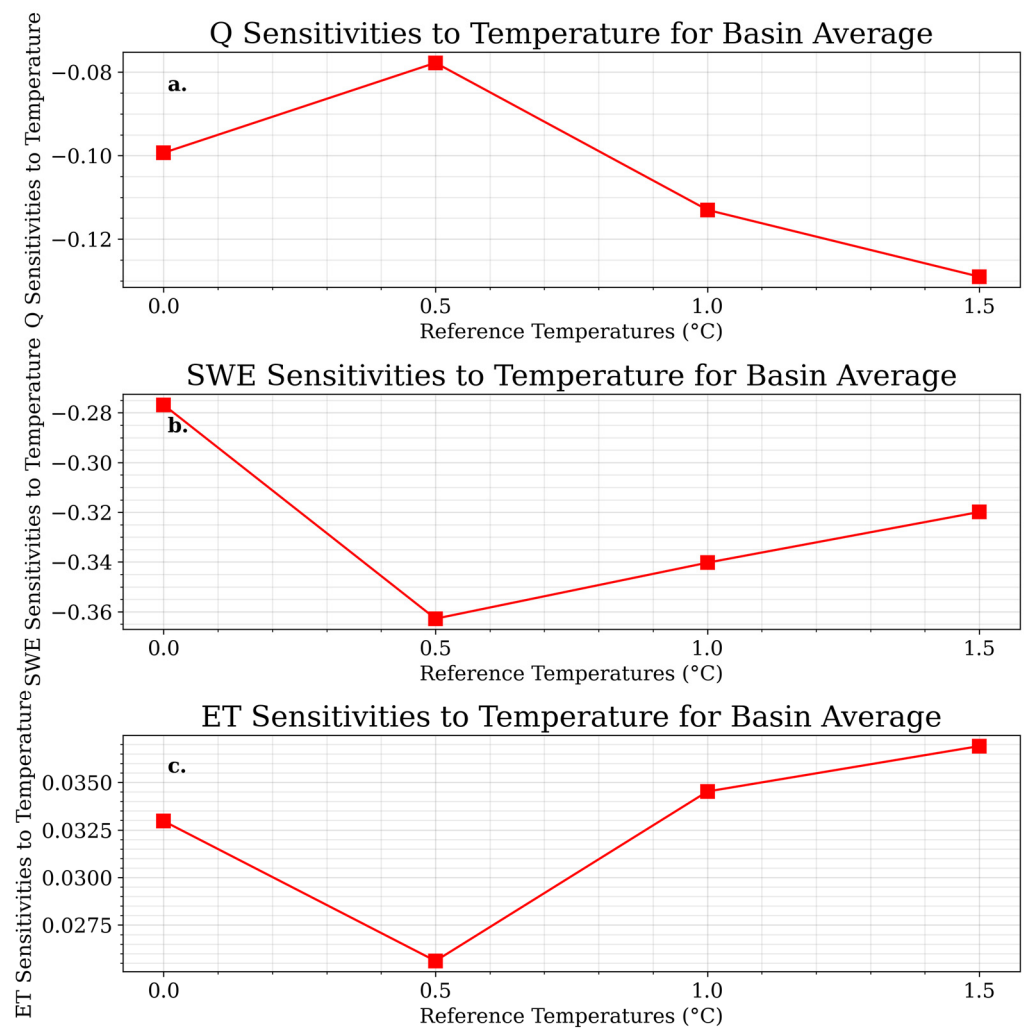

Figure 8. Streamflow, snow water equivalent, and evapotranspiration sensitivities to the precipitation over reference temperatures (0, 0.5, 1, and 1.5 °C) for the basin average. Values on the y-axis are sensitivities. For example, if a Q sensitivity to T is −0.1, each 1 °C increase in temperature results in a 10% reduction in streamflow rates.

The tipping point can be further explored by examining Q sensitivities to T at the monthly scale (Figure 9). Q responds to T positively during the cold season (November–February) since more P will fall as rain, which will contribute to Q faster than snowfall. This response diminishes under warmer reference climates because of less snowpack accumulations. The response of Q to T becomes negative during the warm season (March–

October) and, thus, drives the negative response at the annual scale (Figures 7a and 8a). This response has no significant difference among all reference climate gradience during May–September since any variations in baseline T have little impact on the sensitivity of ET to T because of water limitation. The response of Q to T along the reference T gradient is reversed from March to April; i.e., the warm T has a lower response in March and the opposite in April (Figure 9a). This timing is critical because these are the months for which the primary source of Q shifts from snowmelt to rain, underlining the importance of the snowpack in contributing to this tipping point.
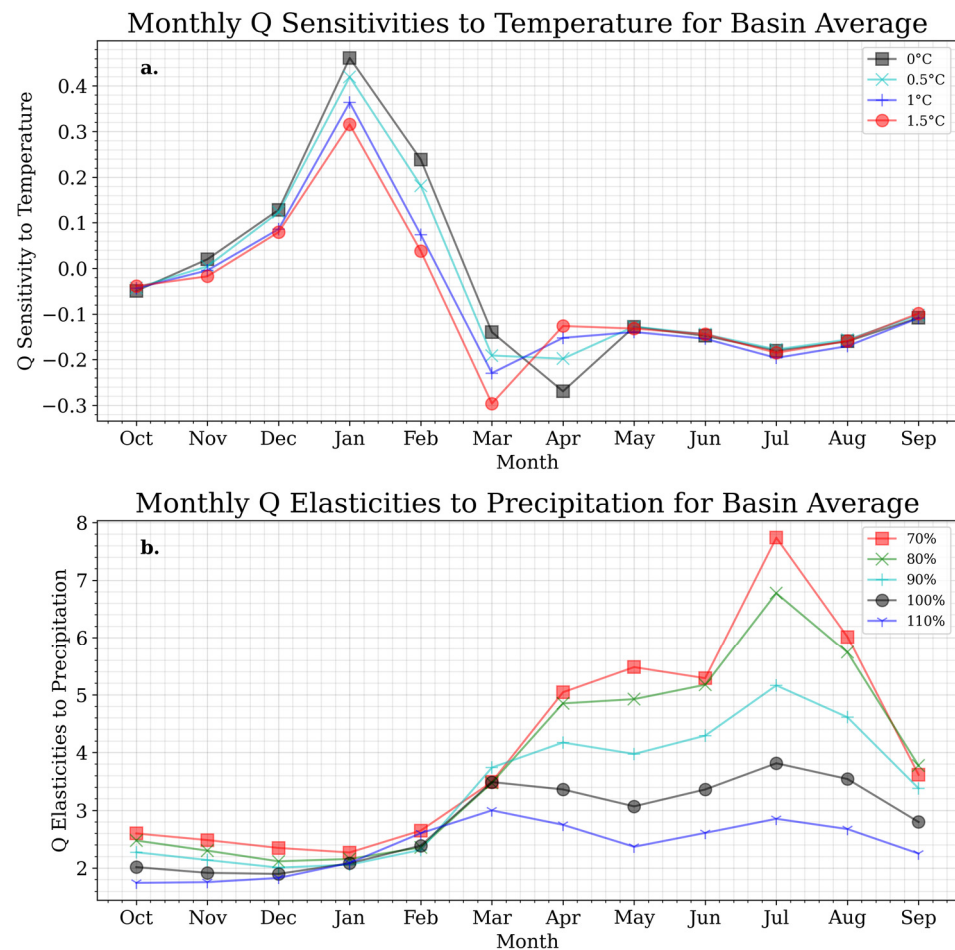

Figure 9. Monthly Q sensitivity to T (**a**) and Q elasticities to P (**b**) for basin-wide averages (Upper Kızılırmak basin) under each reference climate.

3.4. Temperature Perturbation on the Budyko Curve

Figure 10 shows the Budyko curve and the theoretical water and energy limits. A water-limited area is where the ratio of the PET/P is higher than 1, while an energy-limited area is where the ratio of PET/P is lower than 1.

Long-term averages of actual and potential ET and P were calculated from VIC simulations for each reference temperature. As Figure 10 depicts, the points in the Budyko space being calculated from the basin-wide streamflow averages under each reference T scenario are in the area that is water-limited. As the climate becomes warmer, the points move towards the area of drier climate and less runoff.
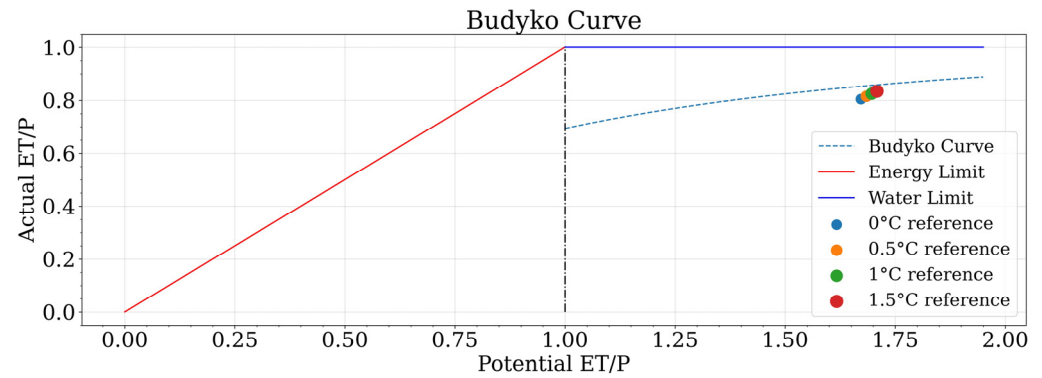
Figure 10. Temperature perturbations on the Budyko curve. All points (from various temperature perturbations) are in the water-limited area. As the reference temperatures increase, the points correspond to drier and lesser water yield areas.

3.5. Coefficients of Variation in Monthly Streamflow

As shown in Figure 11, normally, CVs are higher under drier reference climates in all months (May–September in particular) except for March, and they are higher under warmer climates in the warm season (i.e., May–October), while it is the opposite in the cold season (i.e., January–April). These patterns indicate that the streamflow will become more variable in the summer when the climate is drier and warmer, while during earlier spring, the variation becomes weaker to T perturbations in warmer conditions.
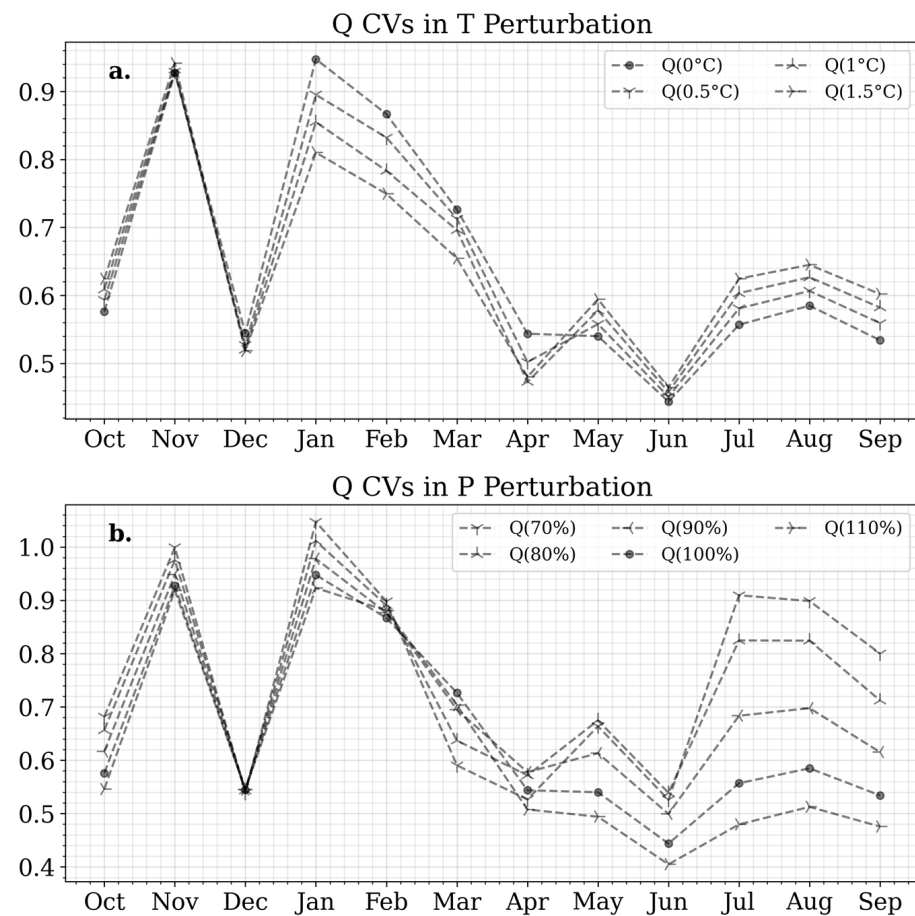

Figure 11. Monthly coefficients of variation under various temperature (**a**) and precipitation (**b**) perturbations.

4. Discussions

4.1. Implications of P and T Elasticities of Q to Water Resource Management

Results from this sensitivity analysis can be summarized in two ways: (1) hydrological responses to each reference climate and (2) hydrological sensitivity to small perturbations. First, in the reference climates, we observed that the decreasing P and rising T would significantly diminish Q, especially in the spring season. The first result means less water availability in the long term in response to climate change. Less water availability is one point of pressure on decision-makers in terms of water management. Secondly, the sensitivity analysis shows that Q responds to T negatively for all reference climates; this response is non-monotonic, with a stronger decrease after a 0.5 °C increase in reference T (see Figure 8). Streamflow sensitivity to precipitation perturbations increases non-linearly as reference P decreases (see Figure 7). Higher sensitivities and elasticities mean more variable Q in response to changing weather conditions. More variable Qs put pressure on water managers. Figure 11 depicts the monthly coefficients of variation (CV) increase under warmer and drier reference climates in summer months. Therefore, the risk of drought may increase in these months. Additionally, flood events also may increase due to the higher streamflow sensitivity to precipitation under the drier reference climates (see Figure 6).

In addition, according to the sensitivity analysis, P is most critical to Q in July because P elasticities are at a peak in this month (Figure 9b). Therefore, any prospective reduction in precipitation during July may lead to heightened insufficiency in water storage within reservoirs when compared to the other months. Q sensitivities to T are more crucial in March because Q decreases more in this month than in other months (see Figure 9a). From the same perspective, since Q starts to peak and fill the reservoirs with snowmelt as of March, the high level of Q reduction in this month may result in insufficient reservoirs in downstream regions.

4.2. Further Consideration

For future research, it is imperative to employ multi-model results due to the inherent structural uncertainties present in single-model frameworks like the VIC model. These uncertainties stem from several model-specific assumptions, such as the treatment of the channel network where water is confined exclusively to channels once it enters and the handling of sub-grid heterogeneity that arises from the model's use of coarse resolution. These assumptions can significantly influence the model's predictions and outputs, underscoring the need for integrating findings from various models to enhance reliability and comprehensiveness in understanding and predicting hydrological and meteorological phenomena.

Some limitations that should be considered in risk assessments may shed light on future studies in the basin. A sensitivity analysis with a higher resolution hydrological model covering the entire KRB could provide more detailed interpretations, taking into account not only the UKRB but also the three important streams, Delice, Gökırmak, and Devres, that feed the main tributary of the KRB. With high-resolution analysis, in addition to calculating the sensitivities across the basin-wide averages, the sensitivities along the basin can show which specific regions in the basin are the more critical. Additionally, only one hydrological model was used in the sensitivity analysis in this study. In risk assessments, model-vs-model analyses will provide a clearer view of critical points. Finally, the 30-year long-term averages are evaluated as in this study; however, daily values, extreme events, or land cover changes should also be considered in risk assessments.

5. Conclusions

The sensitivity analysis of hydrological processes including Q to climate change over the UKRB, a snow-dominant basin, was quantified by using the VIC model driven with perturbed T and P. The significance of increasing T and decreasing P on streamflow in snow-dominant regions was underscored by findings from this study. This study shows that Q decreases when T increases for all warming scenarios (although this sensitivity reveals a non-monotonic response to the reference climates, with the response becoming

more strongly negative after 0.5 °C of warming). The response of Q to P perturbations increases non-linearly as P decreases in the reference climates. These responses result in a twofold setback for water management in this snow-dominant head watershed under these warming and drying scenarios: (1) average streamflow will likely decrease, and (2) streamflow will be more sensitive to hydroclimatic variability in the future warming climate, meaning that water managers will likely need to plan for greater variability of streamflow conditions. Additional research is needed to develop climate change and adaptation strategies that consider both of these changes.

In conclusion, this study underscores the significant impacts of climate-induced temperature increases and precipitation decreases on streamflow within the snow-dominant UKRB. The findings reveal not only a reduction in average streamflow but also an increased sensitivity to hydroclimatic variability, presenting complex challenges for water management in these regions. Given these outcomes, water managers and policymakers must prioritize the development and implementation of robust adaptation strategies. These strategies should not only mitigate the adverse effects observed under various warming scenarios but also enhance the resilience of water resource systems to accommodate increasing variability. Continuing research into these dynamics will be crucial for informed decision-making and effective management of water resources in the face of ongoing climate change.

Appendix A Metrics/Objectives for Calibrating VIC Monthly Streamflow

The automatic calibration is based on the multi-objective complex evolution (MOCOM-UA) global optimization method [56]. Six metrics/objectives are selected to evaluate model performance:

(1) Nash–Sutcliff model efficiency coefficient (NSE):

$$\text{NSE} = 1 - \frac{\sum_{t=1}^{T} \left(Q_m^t - Q_o^t \right)^2}{\sum_{t=1}^{T} \left(Q_o^t - \overline{Q_o} \right)^2} \tag{A1}$$

where $\overline{Qo}$ is the mean of observed discharges, and Q_m^t and Q_o^t are modeled and observed discharge at time t (here, we use monthly time step), respectively.

(2) Nash–Sutcliffe efficiency with logarithmic values (Ln NSE)

To account for the effect of low flows in our evaluation of model performance, we use the logarithmic value of Q_m^t and Q_o^t in Equation (A2).

(3) Relative bias in annual flow

$$\text{RelBias} = \left| \frac{\overline{Q_m}}{\overline{Q_o}} - 1 \right| \tag{A2}$$

$\overline{Q_m}$ and $\overline{Q_o}$ are the average annual modeled flow and observed flow, respectively.

(4)   Coefficient of determination r^2

$$r^2 = \left(\frac{\sum_{t=1}^{T} \left(Q_o^t - \overline{Q_o} \right) \left(Q_m^t - \overline{Q_m} \right)}{\sqrt{\sum_{t=1}^{T} \left(Q_o^t - \overline{Q_o} \right)^2} \sqrt{\sum_{t=1}^{T} \left(Q_m^t - \overline{Q_m} \right)^2}} \right)^2 \tag{A3}$$

(5)   Absolute average peak flow difference (AvgPeakDiff)

$$\text{AvgPeakDiff} = \left| \overline{Q_o^{peak}} - \overline{Q_m^{peak}} \right| \tag{A4}$$

The average peak flow is calculated from the average monthly flow (i.e., the maximum value).

(6)   Root mean square error (RMSE)

$$\text{RMSE} = \sqrt{\frac{\sum_{t=1}^{T} (Q_o^t - Q_m^t)^2}{T}} \tag{A5}$$

The multiple objectives of the calibration are to obtain the Pareto set, that is, solutions that cannot be improved without degrading at least one of the other objectives. To standardize the above matrices, the NSE, Ln NSE, and r^2 metrics are multiplied by -1 (as greater numbers are preferable for these metrics), and the standardized variable is minimized.

Appendix B Perturbations over Reference Climate Data

Tables A1 and A2 detail the adjustments made to temperature (T) and precipitation (P) for each reference climate and the corresponding incremental changes used to calculate Q_{ref} and $Q_{ref+\Delta}$ as per Equations (5) and (6) in the article. Following the same procedure used for streamflow, we also evaluated the precipitation elasticity and temperature sensitivity of snow water equivalent (SWE) and evapotranspiration (ET), denoted as ε_{SWE} and ε_{ET} as well as S_{SWE} and S_{ET}, respectively. This involved substituting Q in Equations (5) and (6) in the article with SWE or ET to compute these variables.

Table A1. Perturbations made to minimum and maximum temperature. VIC was run for each of these reference climates for increments of both 0 °C and 0.1 °C. Running VIC for these incremental changes allowed for an assessment of streamflow sensitivity to temperature for each of the referenceclimates.

Temperature Perturbations for Each Reference Climate	Tmin and Tmax Reference Climate	Incremental Change (Tmin and Tmax)
0 °C	same with obs.	obs. +0.1 °C
0.5 °C	Obs. +0.5 °C	obs. +0.5 °C + 0.1 °C
1 °C	Obs. +1 °C	obs. +1 °C + 0.1 °C
1.5 °C	Obs. +1.5 °C	obs. +1.5 °C + 0.1 °C

Table A2. Perturbations made to precipitation. VIC was run for each of these reference climates for increments of both 0% and 0.1%. Running VIC for these incremental changes allowed for an assessment of streamflow elasticity to precipitation for each of the reference climates.

Precipitation Perturbations for Each Reference Climate	Precipitation Reference Climate	Incremental Change (Prec.)
100%	same with obs.	Obs. × 101%
70%	70% × obs.	Obs. × 71%
80%	80% × obs.	Obs. × 81%
90%	90% × obs.	Obs. × 91%
110%	110% × obs.	Obs. × 111%

References

1. Barnett, T.P.; Adam, J.C.; Lettenmaier, D.P. Potential Impacts of a Warming Climate on Water Availability in Snow-Dominated Regions. *Nature* **2005**, *438*, 303–309. [CrossRef]
2. Mote, P. Trends in Snow Water Equivalent in the Pacific Northwest and Their Climatic Causes. *Geophys. Res. Lett.* **2003**, *30*, 1601. [CrossRef]
3. Mote, P.; Hamlet, A.; Clark, M.; Lettenmaier, D. Declining Mountain Snowpack in Western North America. *Bull. Am. Meteorol. Soc.* **2005**, *86*, 39–49. [CrossRef]
4. Adam, J.C.; Hamlet, A.F.; Lettenmaier, D.P. Implications of Global Climate Change for Snowmelt Hydrology in the Twenty-First Century. *Hydrol. Process.* **2009**, *23*, 962–972. [CrossRef]
5. Christensen, N.S.; Wood, A.W.; Voisin, N.; Lettenmaier, D.P.; Palmer, R.N. The Effects of Climate Change on the Hydrology and Water Resources of the Colorado River Basin. *Clim. Chang.* **2004**, *62*, 337–363. [CrossRef]
6. Clifton, C.F.; Day, K.T.; Luce, C.H.; Grant, G.E.; Safeeq, M.; Halofsky, J.E.; Staab, B.P. Effects of Climate Change on Hydrology and Water Resources in the Blue Mountains, Oregon, USA. *Clim. Serv.* **2018**, *10*, 9–19. [CrossRef]
7. Doulabian, S.; Golian, S.; Toosi, A.S.; Murphy, C. Evaluating the Effects of Climate Change on Precipitation and Temperature for Iran Using RCP Scenarios. *J. Water Clim. Chang.* **2021**, *12*, 166–184. [CrossRef]
8. Zhang, K.; Shalehy, M.H.; Ezaz, G.T.; Chakraborty, A.; Mohib, K.M.; Liu, L. An Integrated Flood Risk Assessment Approach Based on Coupled Hydrological-Hydraulic Modeling and Bottom-up Hazard Vulnerability Analysis. *Environ. Model. Softw.* **2022**, *148*, 105279. [CrossRef]
9. IPCC. *Climate Change 2021: The Physical Science Basis*; Contribution of Working Group I to the Sixth Assessment Report of the Intergovernmental Panel on Climate Change; Cambridge University Press: Cambridge, UK; New York, NY, USA, 2021.
10. Wilby, R.L.; Dessai, S. Robust Adaptation to Climate Change. *Weather* **2010**, *65*, 180–185. [CrossRef]
11. Hallegatte, S. Strategies to Adapt to an Uncertain Climate Change. *Glob. Environ. Chang.* **2009**, *19*, 240–247. [CrossRef]
12. Brown, C.; Wilby, R.L. An Alternate Approach to Assessing Climate Risks. *Eos Trans. Am. Geophys. Union* **2012**, *93*, 401–402. [CrossRef]
13. Nazemi, A.; Wheater, H.S. Assessing the Vulnerability of Water Supply to Changing Streamflow Conditions. *Eos Trans. Am. Geophys. Union* **2014**, *95*, 288. [CrossRef]
14. Vano, J.A.; Das, T.; Lettenmaier, D.P. Hydrologic Sensitivities of Colorado River Runoff to Changes in Precipitation and Temperature. *J. Hydrometeorol.* **2012**, *13*, 932–949. [CrossRef]
15. Vano, J.A.; Lettenmaier, D.P. A Sensitivity-Based Approach to Evaluating Future Changes in Colorado River Discharge. *Clim. Chang.* **2014**, *122*, 621–634. [CrossRef]
16. Elguindi, N.; Bi, X.; Giorgi, F.; Nagarajan, B.; Pal, J.; Solmon, F.; Rauscher, S.; Zakey, A.; O'Brien, T.; Nogherotto, R. *Regional Climate Model RegCM: Reference Manual Version 4.5*; The Abdus Salam International Centre for Theoretical Physics: Trieste, Italy, 2014; Volume 33.
17. Önol, B.; Bozkurt, D.; Turuncoglu, U.U.; Sen, O.L.; Dalfes, H.N. Evaluation of the Twenty-First Century RCM Simulations Driven by Multiple GCMs over the Eastern Mediterranean–Black Sea Region. *Clim. Dyn.* **2014**, *42*, 1949–1965. [CrossRef]
18. Final Report of the Kizilirmak River Basin. Available online: https://web.archive.org/web/20190828015521/http://iklim.ormansu.gov.tr/ckfinder/userfiles/files/Iklim_Nihai_Rapor_K%C4%B1z%C4%B1l%C4%B1rmak_Ek_17_REV_nihai.pdf (accessed on 28 August 2019).
19. iklimsu. Impact of Climate Change on Water Resources Project. Available online: https://iklimportal.gov.tr/Library/Detail/CfDJ8CuYF_1DddVNnSMW43t05Qf-n4lPr5zpU0lSHwlKucc4ey0MB_b4zwT5P1Ij19rPoBfn1NW8Zw-4EwxcGHSc6GdpQgAMH-K_QSqvLt7yRH2_rtWxlj1u2fy5vfWL_x2hmA?type=CfDJ8CuYF_1DddVNnSMW43t05QcFm1Plqi6h-xCipufv2vEfAFI_SDjyWC9rnmVDmlVJ1FeZqe322BgNef6q2Ir-xVgCh-80zedAS5_-QxF5-8xDfO2tYTKjxJIIeVnWF6cVSw (accessed on 1 January 2024).
20. Tockner, K.; Uehlinger, U.; Robinson, C.T. *Rivers of Europe*, 1st ed.; Academic Press: Amsterdam, The Netherlands, 2009; ISBN 978-0-12-3694.
21. Stocker, T. *Climate Change 2013: The Physical Science Basis: Working Group I Contribution to the Fifth Assessment Report of the Intergovernmental Panel on Climate Change*; Cambridge University Press: Cambridge, UK, 2014; ISBN 1-107-05799-X.
22. Liang, X.; Lettenmaier, D.P.; Wood, E.F.; Burges, S.J. A Simple Hydrologically Based Model of Land Surface Water and Energy Fluxes for General Circulation Models. *J. Geophys. Res. Atmos.* **1994**, *99*, 14415–14428. [CrossRef]
23. Sağdıç, M.; Koç, H. Yukarı Kızılırmak Havzası'nın İklimi. *Türk Coğrafya Derg.* **2012**, *58*, 1–20.
24. DSİ. General Directorate—Streamflow Observation Annuals. Available online: https://web.archive.org/web/20190507074720/http://www.dsi.gov.tr/faaliyetler/akim-gozlem-yilliklari (accessed on 26 June 2019).
25. Sheffield, J.; Goteti, G.; Wood, E.F. Development of a 50-Year High-Resolution Global Dataset of Meteorological Forcings for Land Surface Modeling. *J. Clim.* **2006**, *19*, 3088–3111. [CrossRef]
26. Adam, J.C.; Clark, E.A.; Lettenmaier, D.P.; Wood, E.F. Correction of Global Precipitation Products for Orographic Effects. *J. Clim.* **2006**, *19*, 15–38. [CrossRef]
27. Taylor, K.E.; Stouffer, R.J.; Meehl, G.A. An Overview of CMIP5 and the Experiment Design. *Bull. Am. Meteorol. Soc.* **2011**, *93*, 485–498. [CrossRef]

28. Pachauri, R.K.; Allen, M.R.; Barros, V.R.; Broome, J.; Cramer, W.; Christ, R.; Church, J.A.; Clarke, L.; Dahe, Q.; Dasgupta, P. *Climate Change 2014: Synthesis Report. Contribution of Working Groups I, II and III to the Fifth Assessment Report of the Intergovernmental Panel on Climate Change*; IPCC: Geneva, Switzerland, 2014; ISBN 92-9169-143-7.

29. van Vuuren, D.P.; Edmonds, J.; Kainuma, M.; Riahi, K.; Thomson, A.; Hibbard, K.; Hurtt, G.C.; Kram, T.; Krey, V.; Lamarque, J.-F.; et al. The Representative Concentration Pathways: An Overview. *Clim. Chang.* **2011**, *109*, 5–31. [CrossRef]

30. Liang, X.; Wood, E.F.; Lettenmaier, D.P. Surface Soil Moisture Parameterization of the VIC-2L Model: Evaluation and Modification. *Glob. Planet. Chang.* **1996**, *13*, 195–206. [CrossRef]

31. Nijssen, B.; Lettenmaier, D.P.; Liang, X.; Wetzel, S.W.; Wood, E.F. Streamflow Simulation for Continental-Scale River Basins. *Water Resour. Res.* **1997**, *33*, 711–724. [CrossRef]

32. Andreadis, K.M.; Storck, P.; Lettenmaier, D.P. Modeling Snow Accumulation and Ablation Processes in Forested Environments. *Water Resour. Res.* **2009**, *45*, W05429. [CrossRef]

33. Cherkauer, K.A.; Bowling, L.C.; Lettenmaier, D.P. Variable Infiltration Capacity Cold Land Process Model Updates. *Glob. Planet. Chang.* **2003**, *38*, 151–159. [CrossRef]

34. Bao, Z.; Zhang, J.; Yan, X.; Wang, G.; Jin, J.; Liu, Y.; Guan, X. Future Streamflow Assessment in the Haihe River Basin Located in Northern China Using a Regionalized Variable Infiltration Capacity Model Based on 18 CMIP5 GCMs. *J. Water Clim. Chang.* **2020**, *11*, 1551–1569. [CrossRef]

35. Elsner, M.M.; Cuo, L.; Voisin, N.; Deems, J.S.; Hamlet, A.F.; Vano, J.A.; Mickelson, K.E.B.; Lee, S.-Y.; Lettenmaier, D.P. Implications of 21st Century Climate Change for the Hydrology of Washington State. *Clim. Chang.* **2010**, *102*, 225–260. [CrossRef]

36. Liu, M.; Adam, J.C.; Richey, A.S.; Zhu, Z.; Myneni, R.B. Factors Controlling Changes in Evapotranspiration, Runoff, and Soil Moisture over the Conterminous U.S.: Accounting for Vegetation Dynamics. *J. Hydrol.* **2018**, *565*, 123–137. [CrossRef]

37. Liu, M.; Adam, J.C.; Hamlet, A.F. Spatial-Temporal Variations of Evapotranspiration and Runoff/Precipitation Ratios Responding to the Changing Climate in the Pacific Northwest during 1921–2006. *J. Geophys. Res.* **2013**, *118*, 380–394. [CrossRef]

38. Nijssen, B.; O'Donnell, G.M.; Hamlet, A.F.; Lettenmaier, D.P. Hydrologic Sensitivity of Global Rivers to Climate Change. *Clim. Chang.* **2001**, *50*, 143–175. [CrossRef]

39. Schaperow, J.R.; Li, D.; Margulis, S.A.; Lettenmaier, D.P. A Near-Global, High-Resolution Land Surface Parameter Dataset for the Variable Infiltration Capacity Model. *Sci. Data* **2021**, *8*, 216. [CrossRef] [PubMed]

40. Abughali, B.J. Parametrization of Crop Models Using UAS Captured Data. Master's Thesis, Purdue University, West Lafayette, IN, USA, 2021. [CrossRef]

41. Karimi, T.; Reed, P.; Malek, K.; Adam, J. Diagnostic Framework for Evaluating How Parametric Uncertainty Influences Agro-Hydrologic Model Projections of Crop Yields Under Climate Change. *Water Resour. Res.* **2022**, *58*, e2021WR031249. [CrossRef]

42. Malek, K.; Adam, J.C.; Stöckle, C.O.; Peters, R.T. Climate Change Reduces Water Availability for Agriculture by Decreasing Non-Evaporative Irrigation Losses. *J. Hydrol.* **2018**, *561*, 444–460. [CrossRef]

43. Malek, K.; Stöckle, C.; Chinnayakanahalli, K.; Nelson, R.; Liu, M.; Rajagopalan, K.; Barik, M.; Adam, J.C. VIC–CropSyst-v2: A Regional-Scale Modeling Platform to Simulate the Nexus of Climate, Hydrology, Cropping Systems, and Human Decisions. *Geosci. Model Dev.* **2017**, *10*, 3059–3084. [CrossRef]

44. Demaria, E.M; Nijssen, B.; Wagener, T. Monte Carlo Sensitivity Analysis of Land Surface Parameters Using the Variable Infiltration Capacity Model. *J. Geophys. Res. Atmos.* **2007**, *112*, D11113. [CrossRef]

45. Gou, J.; Miao, C.; Duan, Q.; Tang, Q.; Di, Z.; Liao, W.; Wu, J.; Zhou, R. Sensitivity Analysis-Based Automatic Parameter Calibration of the VIC Model for Streamflow Simulations Over China. *Water Resour. Res.* **2020**, *56*, e2019WR025968. [CrossRef]

46. Sepúlveda, U.; Mendoza, P.A.; Mizukami, N.; Newman, A.J. Revisiting Parameter Sensitivities in the Variable Infiltration Capacity Model across a Hydroclimatic Gradient. *Hydrol. Earth Syst. Sci.* **2022**, *26*, 3419–3445. [CrossRef]

47. Umair, M.; Kim, D.; Ray, R.L.; Choi, M. Estimating Land Surface Variables and Sensitivity Analysis for CLM and VIC Simulations Using Remote Sensing Products. *Sci. Total Environ.* **2018**, *633*, 470–483. [CrossRef] [PubMed]

48. Vano, J.A. Hydrologic Sensitivities of Western U.S. Rivers to Climate Change. Ph.D. Thesis, University of Washington, Seattle, WA, USA, 2013.

49. Nijssen, B.; O'Donnell, G.M.; Lettenmaier, D.P.; Lohmann, D.; Wood, E.F. Predicting the Discharge of Global Rivers. *J. Clim.* **2001**, *14*, 3307–3323. [CrossRef]

50. Nijssen, B.; Schnur, R.; Lettenmaier, D.P. Global Retrospective Estimation of Soil Moisture Using the Variable Infiltration Capacity Land Surface Model, 1980–93. *J. Clim.* **2001**, *14*, 1790–1808. [CrossRef]

51. Myneni, R.B.; Ramakrishna, R.; Nemani, R.; Running, S.W. Estimation of Global Leaf Area Index and Absorbed Par Using Radiative Transfer Models. *IEEE Trans. Geosci. Remote Sens.* **1997**, *35*, 1380–1393. [CrossRef]

52. Sheffield, J.; Wood, E.F. Characteristics of Global and Regional Drought, 1950–2000: Analysis of Soil Moisture Data from off-line Simulation of the Terrestrial Hydrologic Cycle. *J. Geophys. Res. Atmos.* **2007**, *112*, D17115. [CrossRef]

53. Khan, N.; Sachindra, D.A.; Shahid, S.; Ahmed, K.; Shiru, M.S.; Nawaz, N. Prediction of Droughts over Pakistan Using Machine Learning Algorithms. *Adv. Water Resour.* **2020**, *139*, 103562. [CrossRef]

54. Müller Schmied, H.; Cáceres, D.; Eisner, S.; Flörke, M.; Herbert, C.; Niemann, C.; Peiris, T.A.; Popat, E.; Portmann, F.T.; Reinecke, R.; et al. The Global Water Resources and Use Model WaterGAP v2.2d: Model Description and Evaluation. *Geosci. Model Dev.* **2021**, *14*, 1037–1079. [CrossRef]

55. Bierkens, M.F.P. Global Hydrology 2015: State, Trends, and Directions. *Water Resour. Res.* **2015**, *51*, 4923–4947. [CrossRef]

56. Yapo, P.O.; Gupta, H.V.; Sorooshian, S. Multi-Objective Global Optimization for Hydrologic Models. *J. Hydrol.* **1998**, *204*, 83–97. [CrossRef]
57. Maurer, E.P.; Wood, A.W.; Adam, J.C.; Lettenmaier, D.P.; Nijssen, B. A Long-Term Hydrologically Based Dataset of Land Surface Fluxes and States for the Conterminous United States. *J. Clim.* **2002**, *15*, 3237–3251. [CrossRef]
58. Nash, J.E.; Sutcliffe, J.V. River Flow Forecasting through Conceptual Models Part I—A Discussion of Principles. *J. Hydrol.* **1970**, *10*, 282–290. [CrossRef]
59. Singh, J.; Knapp, H.V.; Arnold, J.G.; Demissie, M. Hydrological Modeling of the Iroquois River Watershed Using HSPF and Swat. *JAWRA J. Am. Water Resour. Assoc.* **2005**, *41*, 343–360. [CrossRef]
60. Déry, S.J.; Sheffield, J.; Wood, E.F. Connectivity between Eurasian Snow Cover Extent and Canadian Snow Water Equivalent and River Discharge. *J. Geophys. Res. Atmos.* **2005**, *110*, D23106. [CrossRef]
61. Kang, D.H.; Shi, X.; Gao, H.; Déry, S.J. On the Changing Contribution of Snow to the Hydrology of the Fraser River Basin, Canada. *J. Hydrometeorol.* **2014**, *15*, 1344–1365. [CrossRef]
62. Budyko, M.I.; Miller, D.H.; Miller, D.H. *Climate and Life*; Academic Press: New York, NY, USA, 1974; Volume 508.
63. Yang, D.; Sun, F.; Liu, Z.; Cong, Z.; Ni, G.; Lei, Z. Analyzing Spatial and Temporal Variability of Annual Water-Energy Balance in Nonhumid Regions of China Using the Budyko Hypothesis. *Water Resour. Res.* **2007**, *43*, W04426. [CrossRef]
64. Wang, C.; Wang, S.; Fu, B.; Zhang, L. Advances in Hydrological Modelling with the Budyko Framework: A Review. *Prog. Phys. Geogr. Earth Environ.* **2016**, *40*, 409–430. [CrossRef]
65. Adam, J.C.; Lettenmaier, D.P. Adjustment of Global Gridded Precipitation for Systematic Bias. *J. Geophys. Res. Atmos.* **2003**, *108*, 4257. [CrossRef]
66. Moriasi, D.N.; Arnold, J.G.; van Liew, M.W.; Bingner, R.L.; Harmel, R.D.; Veith, T.L. Veith Model Evaluation Guidelines for Systematic Quantification of Accuracy in Watershed Simulations. *Trans. ASABE* **2007**, *50*, 885–900. [CrossRef]